Supporting Information

Reversible Transformation between $Au_{14}Ag_8$ and $Au_{14}Ag_4$ Nanoclusters

Peiyao Pan,[a,b,‡] Chuanjun Zhou,[a,b,‡] Hao Li,[a,b] Chen Zhu,[a,b] Cheng Chen,[c] Xi Kang,[a,b,*] Manzhou Zhu[a,b,*]

[a]Department of Chemistry and Centre for Atomic Engineering of Advanced Materials, Anhui Province Key Laboratory of Chemistry for Inorganic/Organic Hybrid Functionalized Materials, Anhui University, Hefei 230601, P. R. China.

[b]Key Laboratory of Structure and Functional Regulation of Hybrid Materials, Anhui University, Ministry of Education, Hefei 230601, P. R. China.

[c]Institutes of Physical Science and Information Technology, Anhui University, Hefei, Anhui 230601, P. R. China.

[‡]These authors contributed equally to this work.

*E-mails of corresponding authors: kangxi_chem@ahu.edu.cn (X.K.); zmz@ahu.edu.cn (M.Z.).

Notes: The authors declare no competing financial interest.

This Supporting Information includes:

Figures S1-S11

Tables S1-S3

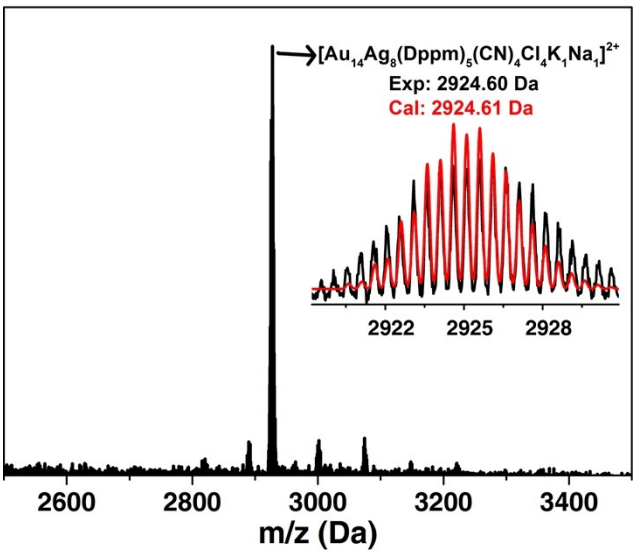

Fig. S1 ESI-MS result of the $Au_{14}Ag_8(Dppm)_6(CN)_4Cl_4$ nanocluster in the positive mode. Inset: the experimental (black line) and the calculated isotope (red line) patterns. As determined by the mass spectrometry, the valence state of the nanocluster is +2, i.e., $[Au_{14}Ag_8(Dppm)_5(CN)_4Cl_4K_1Na_1]^{2+}$.

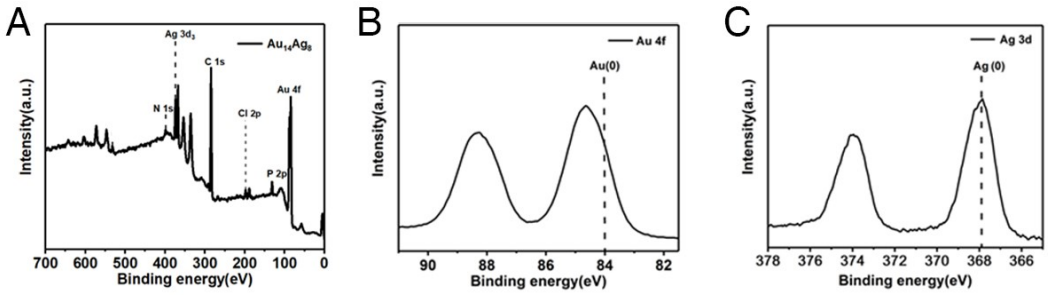

Fig. S2 XPS results of the $Au_{14}Ag_8(Dppm)_6(CN)_4Cl_4$ nanocluster. (A) Full spectrum; (B) Au 4f spectrum; (C) Ag 3d spectrum.

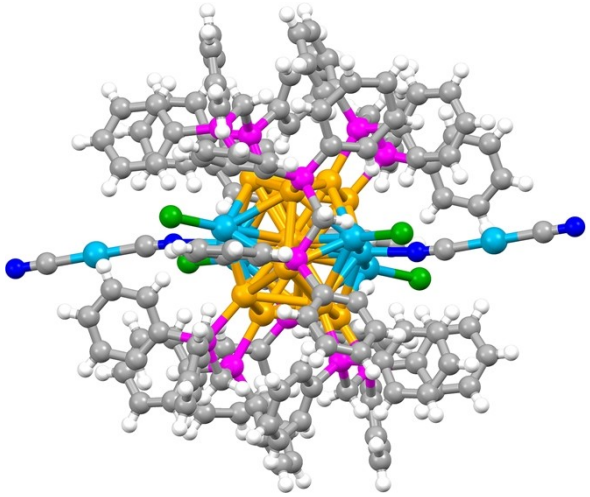

Fig. S3 Overall structure of the $Au_{14}Ag_8(Dppm)_6(CN)_4Cl_4$ nanocluster.

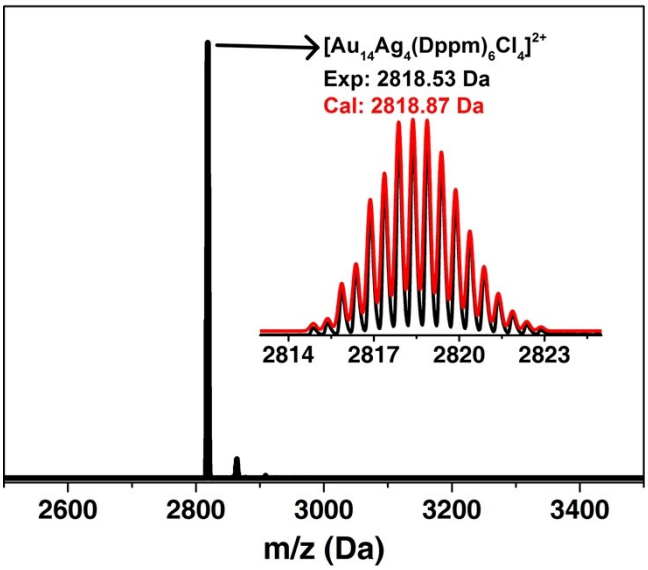

Fig. S4 ESI-MS result of the $Au_{14}Ag_4(Dppm)_6Cl_4$ nanocluster in the positive mode. Inset: the experimental (black line) and the calculated isotope (red line) patterns. As determined by the mass spectrometry, the valence state of the nanocluster is +2, i.e., $[Au_{14}Ag_4(Dppm)_6Cl_4]^{2+}$.

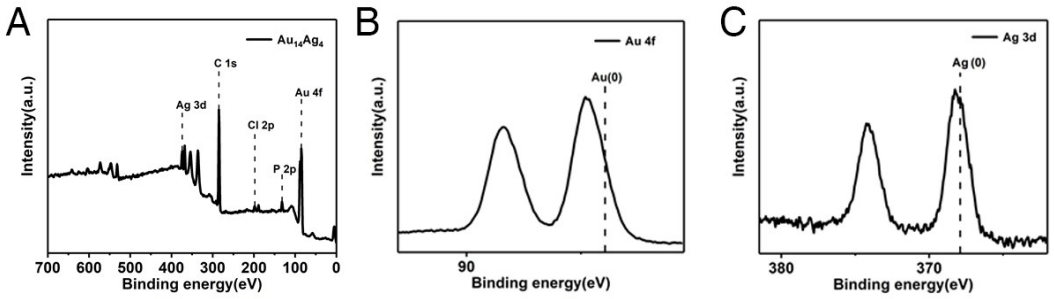

Fig. S5 XPS results of the $Au_{14}Ag_4(Dppm)_6Cl_4$ nanocluster. (A) Full spectrum; (B) Au 4f spectrum; (C) Ag 3d spectrum.

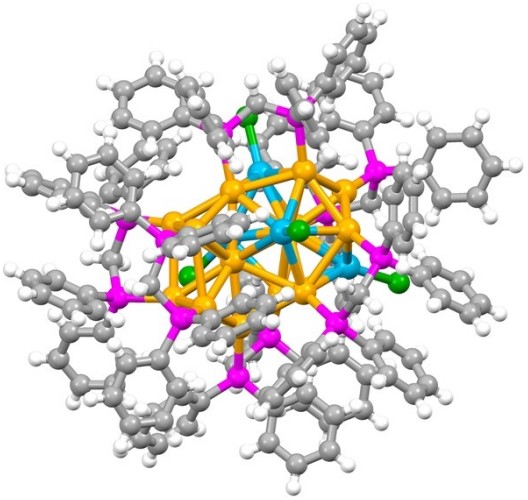

Fig. S6 Overall structure of the $Au_{14}Ag_4(Dppm)_6Cl_4$ nanocluster.

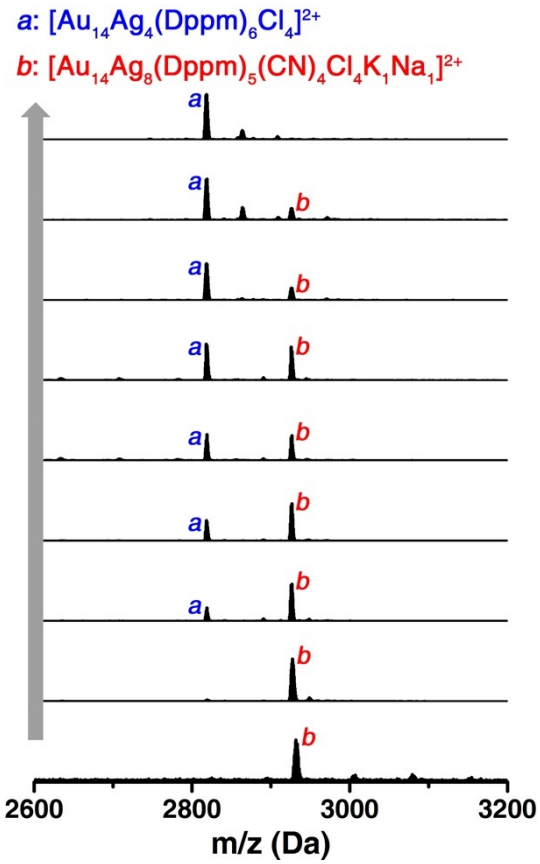

Fig. S7 ESI-MS results of the nanocluster transformation from $Au_{14}Ag_8(Dppm)_6(CN)_4Cl_4$ to $Au_{14}Ag_4(Dppm)_6Cl_4$. *a*: mass signal of $[Au_{14}Ag_4(Dppm)_6Cl_4]^{2+}$; *b*: mass signal of $[Au_{14}Ag_8(Dppm)_5(CN)_4Cl_4K_1Na_1]^{2+}$.

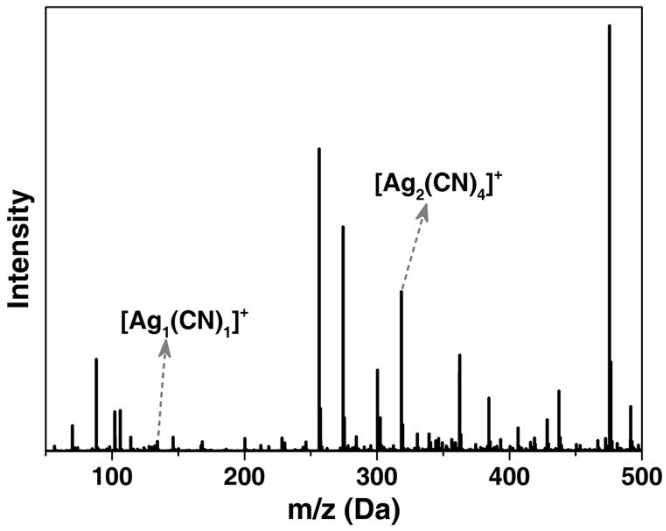

Fig. S8 ESI-MS results of the transformation from $Au_{14}Ag_8(Dppm)_6(CN)_4Cl_4$ to $Au_{14}Ag_4(Dppm)_6Cl_4$ to detect the eliminated species along with the cluster transformation. Two special mass peaks (i.e., 132.90 and 319.82 Da) in the range from 50 to 500 Da were observed, corresponding to $[Ag_1(CN)_1]^+$ and $[Ag_2(CN)_4]^+$, respectively.

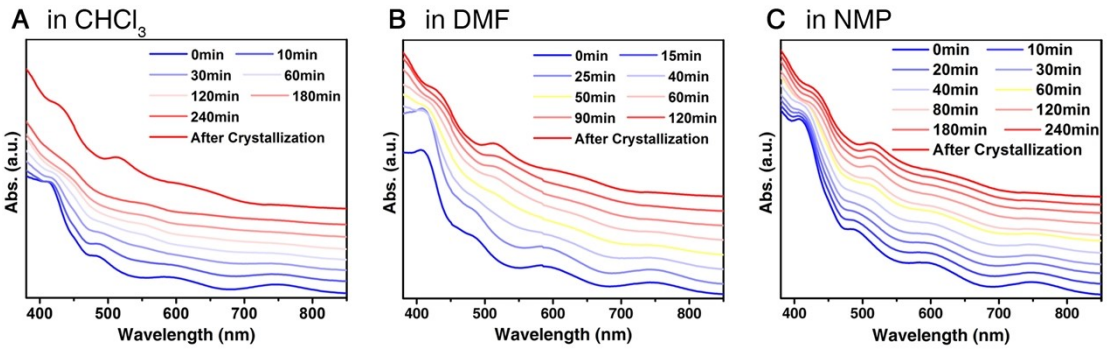

Fig. S9 Time-dependent optical absorptions for the nanocluster transformation from $Au_{14}Ag_8(Dppm)_6(CN)_4Cl_4$ to $Au_{14}Ag_4(Dppm)_6Cl_4$ in (A) $CHCl_3$, (B) DMF, and (C) NMP.

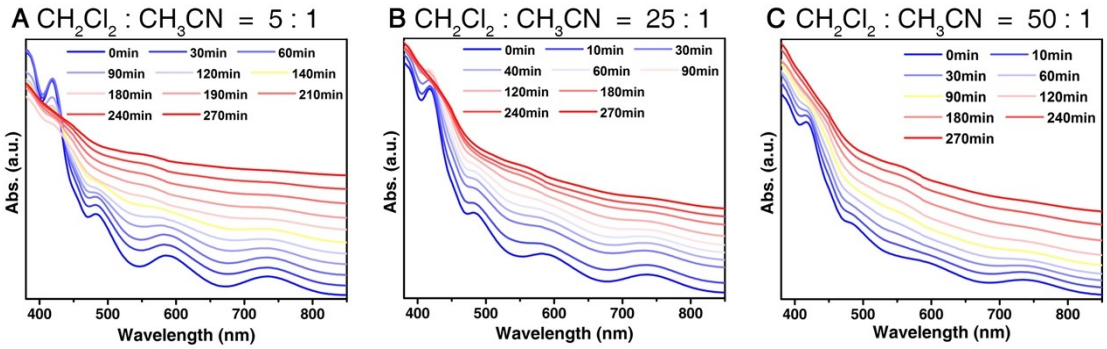

Fig. S10 Time-dependent optical absorptions for the nanocluster transformation from $Au_{14}Ag_8(Dppm)_6(CN)_4Cl_4$ to $Au_{14}Ag_4(Dppm)_6Cl_4$ in different mixed solvents including (A) CH_2Cl_2:CH_3CN = 5:1, (B) CH_2Cl_2:CH_3CN = 25:1, and (C) CH_2Cl_2:CH_3CN = 50:1.

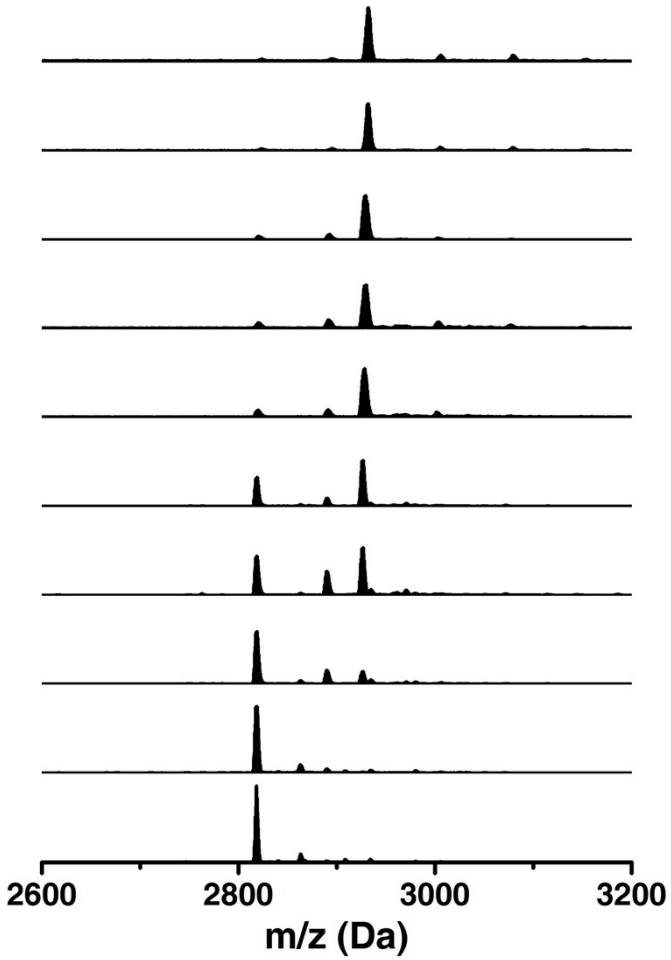

Fig. S11 ESI-MS results of the nanocluster transformation from $Au_{14}Ag_4(Dppm)_6Cl_4$ to $Au_{14}Ag_8(Dppm)_6(CN)_4Cl_4$. *a*: mass signal of $[Au_{14}Ag_4(Dppm)_6Cl_4]^{2+}$; *b*: mass signal of $[Au_{14}Ag_8(Dppm)_5(CN)_4Cl_4K_1Na_1]^{2+}$; *c*: mass signal of $[Au_{14}Ag_6(Dppm)_6Cl_2]^{2+}$.

Table S1. Atom ratio of Au and Ag in $Au_{14}Ag_8(Dppm)_6(CN)_4Cl_4$ and $Au_{14}Ag_4(Dppm)_6Cl_4$ nanoclusters. Atom ratios of Au and Ag in both nanoclusters were calculated from X-ray photoelectric spectroscopy (XPS).

$Au_{14}Ag_8(Dppm)_6(CN)_4Cl_4$	Au atom	Ag atom
XPS Experiment Ratio	62.85%	37.15%
Theoretical Ratio	63.64%	36.36%

$Au_{14}Ag_4(Dppm)_6Cl_4$	Au atom	Ag atom
XPS Experiment Ratio	77.15%	22.85%
Theoretical Ratio	77.78%	22.22%

Table S2. Crystal data and structure refinement for the $Au_{14}Ag_4(Dppm)_6Cl_4$ nanocluster. CCDC number is 2094995.

Crystal system	monoclinic
Space group	$P\,2_1/n$
a/Å	16.4329(2)
b/Å	56.1369(8)
c/Å	18.7093(3)
α/°	90
β/°	99.7170(10)
γ/°	90
Volume/Å^3	17011.6(4)
Z	4
ρcalcg/cm^3	2.229
μ/mm^{-1}	27.910
F(000)	10432
Radiation	CuKα (λ = 1.54186)
Index ranges	-6 ≤ h ≤ 18, -64 ≤ k ≤ 59, -21 ≤ l ≤ 20
Final R indexes [I>=2σ (I)]	R1 = 0.0706, wR2 = 0.1936
Final R indexes [all data]	R1 = 0.0816, wR2 = 0.2095

Table S3. Crystal data and structure refinement for the $Au_{14}Ag_8(Dppm)_6(CN)_4Cl_4$ nanocluster. CCDC number is 2094999.

Crystal system	monoclinic
Space group	$P\ 2_1/c$
a/Å	17.3969(5)
b/Å	23.5948(4)
c/Å	23.5308(5)
α/°	90
β/°	90.862(2)
γ/°	90
Volume/$Å^3$	9657.7(4)
Z	2
ρcalcg/cm^3	2.123
μ/mm^{-1}	27.508
F(000)	5628
Radiation	CuKα (λ = 1.54186)
Index ranges	-20 ≤ h ≤ 19, -27 ≤ k ≤ 22, -27 ≤ l ≤ 19
Final R indexes [I>=2σ (I)]	R1 = 0.0927, wR2 = 0.2556
Final R indexes [all data]	R1 = 0.1217, wR2 = 0.2844

Three Level B Alerts exist, resulting from the disorder of peripheral ligands of the nanocluster. However, the structure and the composition of this nanocluster are correct since several supplementary approaches, including ESI-MS and XPS, have been performed to confirm the crystal structure of the $Au_{14}Ag_8(Dppm)_6(CN)_4Cl_4$ nanocluster.